Design of a High-Efficiency Low-Voltage Axially Modulated Cusp-Injected Second-Harmonic X-Band Gyrotron Amplifier

Wes Lawson, *Senior Member, IEEE,* A. Grigoropoulos, A. Liu, Girish P. Saraph, *Member, IEEE,* John Rodgers, and William W. Destler, *Fellow, IEEE*

***Abstract*— We present the theoretical design of a second-harmonic small-orbit gyrotron amplifier which utilizes the interaction between a 35-kV 4-A beam and a TE_{011} cavity to produce over 70 kW of amplified power at 9.9 GHz in a 1.83-kG magnetic field. One of the novel features of this device is that the electron gun produces an axially streaming annular beam which is velocity modulated by a short TM_{0n0} input cavity. Perpendicular energy is imparted to the beam via a nonadiabatic magnetic transition at the end of a 13-cm drift region. An electronic efficiency of 53% is predicted with a large signal gain near 20 dB by a single particle code which takes into account nonideal effects associated with finite beam thickness and finite magnetic field transition widths.**

I. Introduction

IN RECENT years, numerous theoretical and experimental investigations of gyrotrons operating near the fundamental cyclotron frequency have proven them to be reliable efficient high-power sources of microwave and millimeter wave radiation [1]–[4]. These studies have been performed over a wide range of parameters and have resulted in a wealth of information about the electron gun requirements and characteristics and about the stability, efficiency, and mode competition properties of microwave circuits for gyrotrons [5]–[9]. Potential applications of these sources include RF drivers for accelerators, plasma heating in magnetic fusion research, millimeter wave and deep space radar, materials processing, and nonlinear spectroscopy of semiconductors and biological materials.

Unfortunately, conventional gyrotrons operating near the fundamental cyclotron frequency (first-harmonic gyrotrons) must be immersed in a magnetic field whose strength is linearly proportional to the output frequency. Thus, they are not viable candidates for some high-frequency applications that require compact and lightweight tubes. Two potential ways to decrease the applied magnetic field and the accompanying material bulk and power consumption are to 1) use Doppler upshifting via operation at a high axial wavenumber and 2) operate at a harmonic of the cyclotron frequency. The cyclotron auto-resonance maser (CARM) is an example of a device that takes the first approach. Many CARM's have been built and tested, but none have come close to the efficiencies achieved in first-harmonic gyrotrons [10]–[12]. Mode competition from gyrotron instabilities and sensitivity to velocity spread have typically been the limiting factors. Low-harmonic operation (typically the second or third harmonic) has met with some success in the conventional small-orbit gyrotron configuration [13]–[16] and high-harmonic devices have been fairly successful in the large-orbit configuration [17]–[33]. Still, the efficiencies of second-harmonic devices usually lag behind their first-harmonic counterparts by several percent and efficiencies tend to decrease fairly rapidly with increasing harmonic number after that point.

We have recently proposed [34] a method of prebunching the electron beam to enhance the efficiency in high-harmonic large-orbit devices which is based on the cusp-injection scheme [35]. Before the annular beam passes through the balanced nonadiabatic magnetic field reversal, it first encounters a circularly polarized TM_{mn0} mode input cavity and a subsequent drift region. The resultant ballistic bunching (potentially) sets up a beam that can efficiently interact at the mth harmonic with a simple right-circular output cavity. For example, the design study in [34] demonstrated that an efficiency of 40% was achievable in X-band at the fourth harmonic via an interaction between a 100-kV 25-A electron beam and a TE_{411} cavity.

While this initial result is quite promising, there are some practical limits to the applicable range of parameters for this device. For example, the beam radius of the large-orbit configuration is equal to the Larmor radius, which is proportional to the perpendicular velocity for a given cyclotron frequency. Thus, the beam radius in low-voltage systems decreases fairly substantially with decreasing beam energy. However, the relative radius of the maximum electric field in a cavity increases with increasing harmonic number. In fact, the electric field at radii much less than the maximum field radius varies by a factor that is proportional to the power of the harmonic number. In such systems, the achievement of the necessary field strength for efficient interaction often leads to unrealistic requirements on output cavity quality factors.

There are at least two possible ways to overcome these difficulties and design efficient low-voltage harmonic devices. One way is to use a vane-resonator to couple various azimuthal modes together. The resultant cavity modes can support the necessary azimuthal field variation with a much lower cutoff

Manuscript received July 12, 1995; revised January 26, 1996. This work was supported by the Tri-Services Program for Vacuum Electronics.

The authors are with the Electrical Engineering Department and Institute for Plasma Research, University of Maryland, College Park, MD 20742 USA (e-mail: lawson@eng.umd.edu).

Publisher Item Identifier S 0093-3813(96)04655-3.

frequency. Thus, the wall radius can be reduced considerably as compared to the smooth wall case and the interaction impedance can be significantly increased. There are some potential drawbacks to this approach. For example, the mode composition of the output signal in an axially coupled vane resonator cavity can be significantly more complicated than for the smooth wall case. Still, this approach has been used with reasonable success in many conventional large-orbit gyrotrons [21], [24], [26], [33]. The design of an axially bunched low-voltage large-orbit gyrotron with a vane resonator will be the subject of a later study.

The approach we will investigate in this work is to prebunch a small-orbit beam. Axial modulation is still a viable concept because a small orbit beam can be generated by a nonadiabatic magnetic transition that does not reverse the direction of the field [36]. The guiding center radius can be adjusted to place the beam at a location where the electric field is relatively strong. This nonzero guiding center radius expands the number of potential modes with which the beam can interact. While this may enable us to select a desirable output mode, it also can potentially lead to additional mode competition problems. A properly prebunched beam, however, should help to reduce mode competition by preferentially selecting the desired operating mode.

We will illustrate this approach via the presentation of a second-harmonic small-orbit system design. In this design, a 35-kV 4-A beam is prebunched by a TM_{020} cavity and interacts with a TE_{011} cavity to theoretically produce over 70 kW of power with an efficiency and large-signal gain of approximately 53% and 20 dB, respectively. In Section II, we discuss the basic amplifier configuration and describe the computer codes used in the analysis. In Section III, we detail the results of the design example and present tube stability and large-signal characteristics. We also characterize the sensitivity of the device to parameter variations. The results of this study are summarized in the final section.

II. Theoretical Model

A simplified schematic of an axially modulated cusp-injected small-orbit gyrotron amplifier is given in Fig. 1(a). A linearly streaming thin mono-energetic annular beam is immersed in a uniform axial magnetic field and injected into a short buncher cavity. The axial electric field of the input cavity [Fig. 1(c)] modulates the energy of the electron beam which results in ballistic bunching as the electrons drift through the region immediately following the cavity (similar to a klystron [37]). When the electrons encounter the nonadiabatic magnetic field transition [shown in Fig. 1(b)], the radial magnetic field produces a Lorentz force which converts part of each electron's energy into perpendicular motion. Because this conversion occurs in a short distance, the electron bunches that form begin to rotate with the particles. These bunches then interact with the electric field in the output cavity [Fig. 1(c)] and, if properly formed, can give up most of their energy to the electromagnetic wave.

In order for the bunches to interact effectively with the output cavity fields, the resonant frequencies of the input

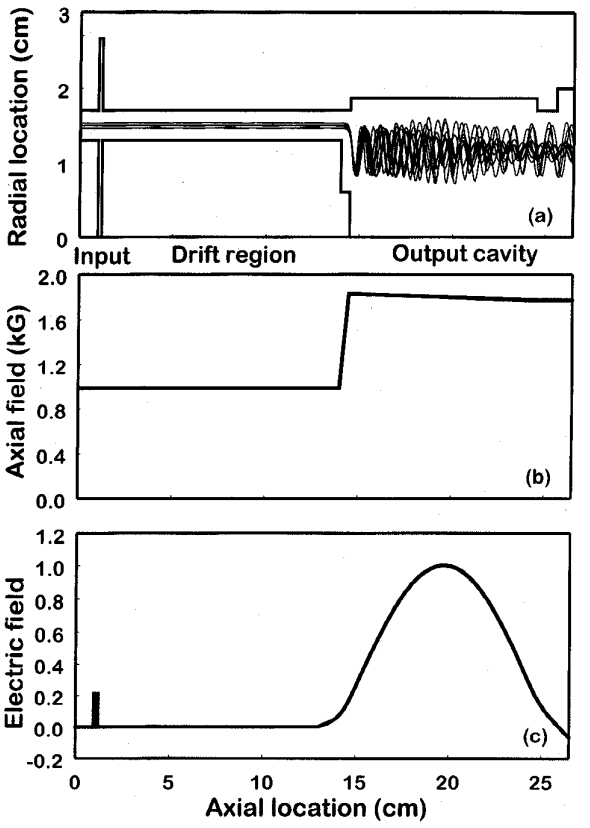

Fig. 1. The axially modulated cusp-injected small-orbit gyrotron: (a) system schematic, (b) axial magnetic field profile, and (c) normalized electric field profile at the beam radius (E_z in the input cavity and E_ϕ in the output cavity).

and output cavities must be nearly integer multiples of the cyclotron frequency (in the output cavity). Furthermore, if s_1 and s_2 are the multiples (harmonics) of the cyclotron frequency in the input and output cavities, respectively, and m_1 and m_2 are the azimuthal mode indexes of the same two cavities, respectively, then the following condition must be satisfied:

$$m_1/s_1 = m_2/s_2. \tag{1}$$

The designs in this work utilize operating modes with $m_1 = m_2 = 0$, so that any combination of s_1 and s_2 are acceptable. We will always focus on the $s_2 = 2$ case. Most of the analysis will be performed with $s_1 = 2$ as well, but we will demonstrate toward the end that an $s_1 = 1$ design is nearly as effective as the earlier design and has several nice features that warrant consideration.

Because the input cavity operates in the TM_{0n0} mode, it can be excited either by a single aperture on the radial wall fed by a standard waveguide or by a single loop fed by a simple coaxial line. The required drift tube length d depends on the magnitude of the energy spread ($\Delta E/E_o$) imparted to the beam and has been derived elsewhere for a low-voltage system as [34]

$$d = \beta_o \lambda/(2\Delta E/E_o) \tag{2}$$

where β_o is the streaming velocity (normalized to the speed of light) and λ is the RF wavelength (of the input cavity signal).

The magnetic transition at the end of the drift region is shortened by a thin iron pole piece. Long solenoids on either side of the pole piece generate approximately constant axial magnetic fields in each region (B_c on the input side and B_o on the output side). The required mismatch between the magnetic field strengths depends on the beam radius and the desired velocity ratio ($\alpha = v_\perp/v_z$). If the original beam radius is r_o and the Larmor radius after the magnetic transition is r_L, then the ratio for an ideal (zero length) transition is [36]

$$B_c/B_o = 1 - 2r_L/r_o. \tag{3}$$

The beam's energy spread results in velocity spreads after the magnetic transition which can be approximated by [34]

$$\frac{\Delta v_z}{v_{\perp_o}} = \frac{1}{2}[1 + \alpha^2 + \alpha^2(\gamma_o^2 - 1)]\frac{\Delta E}{E_o}$$
$$\frac{\Delta v_\perp}{v_{\perp_o}} = -\frac{1}{2}(\gamma_o^2 - 1)\frac{\Delta E}{E_o} \tag{4}$$

when the effects of the input cavity's magnetic fields are neglected. In (4), γ_o is the relativistic mass factor. For low-voltage beams, the induced perpendicular velocity spread is typically small, but the parallel spread can become quite large. Setting an upper limit on this value often dictates the drift tube length in small-orbit designs via (2).

There are two other contributions to the net velocity spreads. The first is from the electron gun optics and hence is design specific, can typically be kept fairly small, and will not be discussed further. The other contribution comes from the canonical angular momentum of finite thickness beams. This spread can be reduced in small-orbit systems by compressing the beam width [36].

The output cavity for the prebunched small orbit gyrotron is a simple axially coupled right-circular waveguide that is designed to operate at the proper frequency in the TE_{011} mode. The cavity has a long main section and a shorter output lip that has a radius smaller than that required for the operating mode to propagate. The resonant frequency and quality factor (Q) are calculated with a scattering-matrix code [38], [39]. In general, the required cavity Q is far below the resistive Q of a copper cavity, but sufficiently large so that the interaction between the beam and the microwaves occurs predominantly in the main section of the cavity. For this reason, the sinusoidal axial field dependence of a closed cavity is often a good approximation for the open-ended cavity.

Four main computer codes are utilized in the design process. The scattering matrix code is used to design the output cavity and a start-oscillation code [40] is used to check the stability of the output cavity to spurious modes in the absence of beam prebunching by the input cavity. This code assumes that the magnetic field is constant in the output cavity.

The other two codes are single particle codes that numerically integrate the particle motion in the device. The first single particle code simulates the beam's motion through the input cavity, the drift region, and the nonadiabatic magnetic transition. Given the beam parameters, electrons are initially "launched" over a range of axial positions, times, and angles that represent the entirety of phase space (after taking into account any symmetries in the system). The initial velocities of the particles are assumed to be purely axial, but electrons can be started from several radial locations to emulate finite thickness beams. The EM fields are assumed to be confined to the input cavity (leakage fields are neglected). The only field in the drift region is the axial magnetic field, which is assumed to remain constant. The magnetic transition region is simulated with a piecewise linear axial field profile. The Runga–Kutta method is used to start the process and a predictor–corrector scheme is used for the bulk of the numerical integration. Numerical convergence is checked by varying integration step size and the number of particles. Conservation of energy and canonical angular momentum are also checked in regions where there is only a static magnetic field. This code produces the phase space distributions of the electrons at the end of the transition region and calculates various quantities that give the average beam statistics and indicate the effectiveness of the bunching process. The resistive Q of a copper input cavity and the required drive power are also reported. This code is typically iterated, while adjusting the drift region length and the strength of the input field, until satisfactory bunching performance is achieved.

The second code takes the results from the first single particle code and uses the same numerical techniques to calculate the extraction efficiency of the EM wave in the output cavity under steady-state conditions. The code can model either a closed circular cavity or it can accept the output from the scattering matrix code to model open resonator configurations. The magnetic field in the output cavity can be tapered linearly to optimize the interaction. This code is typically iterated, while varying the cavity and magnetic field parameters, until an optimal design is achieved. During each efficiency run, the amplitude and phase of the EM wave are adjusted until maximum efficiency is calculated. In addition to the efficiency, the code reports the required diffractive Q and the resistive Q for a closed right-circular copper cavity. By decreasing the field amplitude in the output cavity toward zero, this code can also be used to calculate the start currents for the various modes in tapered magnetic fields, whether the beam is prebunched or unbunched.

We have also run a separate large signal code to independently verify the efficiency calculations in the output cavity. This code, originally designed for relativistic gyroklystrons [40], is modified to take into account the prebunched beam at the entrance of the output cavity from the first single particle code. The code also assumes the cold cavity field profiles and Q value from the scattering matrix code which includes linear mode conversion at the radial steps in the output cavity. In order to optimize the device efficiency, a two-dimensional (2-D) search, in terms of overall mode amplitude and phase, is carried out. To ensure self-consistency in the calculations, the quality factor required to maintain the steady-state field amplitude is matched with the Q value from the scattering matrix code.

TABLE I
SECOND-HARMONIC AMPLIFIER SYSTEM PARAMETERS

Beam Parameters		
Voltage (kV)	35	
Current (A)	4	
	(before cusp)	(after cusp)
Average radius (cm)	1.50	1.18
Beam thickness (mm)	1.00	7.33
Velocity ratio ($v_\perp/v_z$)	0.00	2.28
Input Cavity		
Drive frequency (GHz)	9.9	
Operating mode	TM_{020}	
Resistive Quality factor (Q)	2800	
Radius (cm)	2.66	
Length (cm)	0.20	
Magnetic Field Parameters		
Buncher magnetic field (kG)	0.985	
Output magnetic field (kG)	1.83	
Cyclotron frequency (GHz)	4.794	
Cusp width (cm)	0.50	
Cavity - cusp spacing (cm)	13	
Output field taper	-3%	
Output cavity		
Output frequency (GHz)	9.9	
Operating mode	TE_{011}	
Diffractive Q	1825	
Resistive Q	28,580	
	(main section)	(cavity lip)
Radius (cm)	1.864	1.70
Length (cm)	10.000	1.09

Details of the results from these simulation codes for the specific designs are given in the following section.

III. DESIGN SIMULATION

The parameters for the second harmonic design are given in Table I. The system is designed to produce microwaves at 9.9 GHz via the interaction between a 35-kV 4-A beam and the microwave circuit. The initial beam radius of 1.5 cm is selected to optimize the interaction with the EM wave in the output cavity while avoiding any beam interception. This beam can be generated with a standard electrode configuration [34]. If a magnetic compression of four were to be utilized, for example, the cathode thickness would be 2 mm, the average emitter radius would be 3 cm, and the required current density would be quite modest at a little over 1 A/cm [2]. The table indicates the pre- and postcompression beam dimensions. The dc space charge depression in the output cavity is less than 3% and is considerably smaller before the magnetic transition. The radial thickness corresponds to an ideal postcusp velocity spread of $\Delta v = 1.9\%$ (if beam width compression is not utilized to reduce this number). The average velocity ratio is somewhat larger than a typical small-orbit system, but is below what is often quoted for cusp-injected large-orbit systems.

The drive cavity is a simple right-circular TM_{020} cavity with the dimensions indicated in the table. The cavity width is selected to give a beam coupling factor [37] of about 0.93. The cavity radius is adjusted to achieve the desired operating frequency. Note that the quality factor quoted includes only the losses in the copper. The actual quality factor, after taking into account the input power coupling, should be about one-half of this value. All drive powers quoted in this paper assume a net input Q of 1400. Any beam loading is neglected. The beam is located between the first null and the second peak of the axial electric field. The required input power could be decreased and the resultant gain increased if the beam could be repositioned on the maximum. The easiest way to accomplish this would undoubtedly be to use a coaxial input cavity. Other possibilities include the introduction of dielectrics into the input cavity or moving the input cavity into the magnetic compression region where the beam radius is larger.

The peak axial magnetic field in the output cavity is determined from the optimization procedure and is such that twice the cyclotron frequency is about 3% lower than the drive frequency. The magnetic field in the input region is about 60 G less than predicted by (3) due to the finite cusp width. The distance between the input cavity and cusp transition is optimized with the numerical codes, but the initial length is chosen from (2) and (4) so that maximal bunching could be achieved with an energy spread and an induced axial velocity spread approximately under 3 and 10%, respectively. The transition width should readily achievable with the aid of one or more iron pole pieces. The optimal magnetic field profile is shown in Fig. 1(b).

The length of the output cavity is varied to maximize efficiency while keeping the required Q less than 5–7% of the resistive Q of a copper cavity. This restriction means that over 93% of the microwave power can be extracted. The cavity radius and lip dimensions are adjusted to produce the required resonant frequency and Q while avoiding beam interception (by the particles that are accelerated during the interaction). The main cavity length is such that particles undergo approximately 11 revolutions inside this region. The azimuthal electric field at the beam radius in the output cavity is shown in Fig. 1(c). The exponential decay in the drift region and the leakage field through the coupling aperture can be seen in the figure.

A second constraint on the output cavity is that it be stable to spurious oscillations. The beam current required to achieve self-oscillation in the output cavity is shown in Fig. 2 as a function of (uniform) magnetic field. It is assumed that no drive power is applied to the input cavity. Curves are plotted for the TE_{011} mode and the TE_{111} mode. The resonant frequency of the fundamental TE_{111} mode is near the cyclotron frequency at 4.87 GHz. The quality factor of the TE_{111} mode is 72. All other modes evaluated are completely stable to currents below 10 A in the magnetic field range indicated. The cavity is expected to be unstable to the operating mode, but stable to the fundamental mode at the design field of 1.83 kG. However, the optimal taper (for efficiency) yields a field at the exit of the output cavity of 1.775 kG. At this field magnitude the fundamental mode is unstable and the operating mode is stable. By using the efficiency code, it can be shown that with the tapered field profile the desired mode is again unstable and the TE_{111} mode is stable.

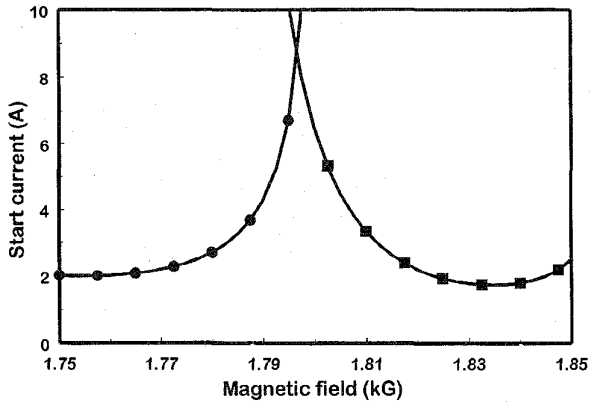

Fig. 2. The output cavity start-oscillation curves. The squares indicate the TE_{011} mode and the circles represent the TE_{111} mode.

The evolution of electron bunching in the device is illustrated in Fig. 3, where the distribution of representative particles relative to the phase of the output cavity's electric field is plotted at various axial locations. Fig. 3(a) represents the distribution just prior to the output cavity when no drive power is applied and illustrates the initially uniform distribution of particles in phase space. The three distinct bands of particles represent the effect of finite beam thickness and the velocity spread that results from canonical angular momentum. Fig. 3(b) shows the distribution at the output cavity entrance when a signal of 800 W is injected into the input cavity. The increase in perpendicular velocity spread can be seen clearly and is comparable (but less than) the canonical angular momentum spread. The phase distribution at the exit of the output cavity which corresponds to the 800 W input case is shown in Fig 3(c). The phase coherence of the beam is essentially destroyed and a large number of particles have given up over 80% of their perpendicular energy. A much smaller number of particles have remained at about the same energy level or had their energy increase slightly. The beam evolution throughout the cavity is indicated in Fig. 1(a) where the r–z projection of representative particles is plotted. The figure reveals that while some particles gain energy and increase their Larmor radii, the majority of the particles lose a significant amount of energy.

The simulated results for the parameters in Table I near the optimal drive power are summarized in Table II. The nominal electric field at the beam is about 8 kV/cm in the input cavity and about five times that in the output cavity. The peak electric field at the wall is 17 kV/cm in the input cavity and zero in the output cavity. The total axial velocity spread includes a contribution of about 8.5% from energy spread, which is reasonably close to the estimate given in (4). The contribution to the perpendicular velocity spread from the energy spread is about 0.8%. The nominal saturated gain is about 20 dB. The peak efficiency of 53% exceeds the performance of any second-harmonic small-orbit amplifier to date.

The dependence of efficiency on output cavity Q is revealed in Fig. 4 for a thin beam and a drive power of 800 W. The output efficiency rises dramatically from ~5% to ~48% as the quality factor is increased from 300 to 1300. After that point,

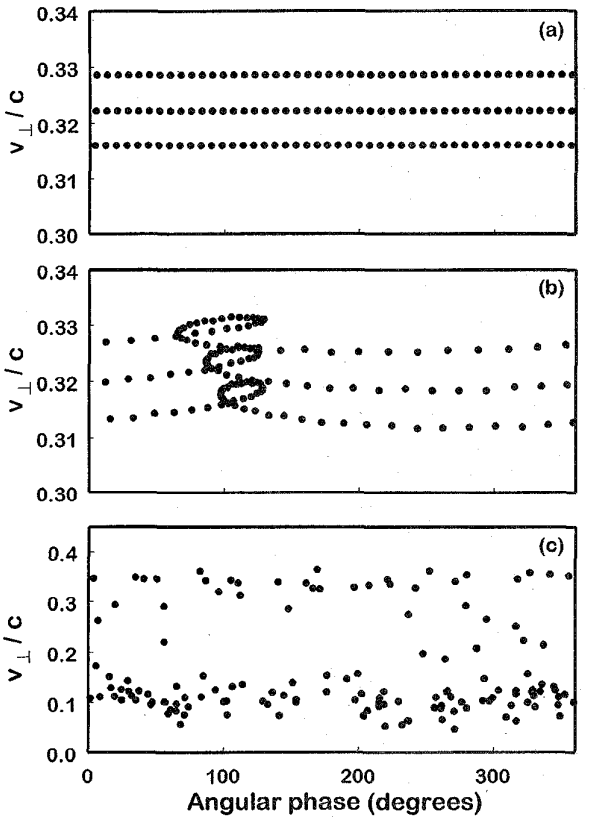

Fig. 3. Representative phase distribution of electrons: (a) output cavity entrance (P_{in} = 0 W), (b) output cavity entrance (P_{in} = 800 W), and (c) output cavity exit (P_{in} = 800 W).

TABLE II
SECOND-HARMONIC AMPLIFIER PERFORMANCE

Input cavity results	
Input drive power (W)	800
E_z at beam (kV/cm)	7.99
Drift region results	
Total Δv_z (%)	12.2
Total $\Delta v_\perp$ (%)	1.8
Energy spread (%)	3.2
Output cavity results	
Power (kW)	74.2
Efficiency (%)	53.0
Gain (dB)	19.7
E_ϕ at beam (kV/cm)	39

the efficiency only increases slowly with Q until it reaches its maximum value of 54.4% when Q = 2550. The nominal Q of 1825 was selected rather than the optimal value because its improved stability and wall loss properties come at only a small sacrifice in efficiency.

Two drive curves for parameters near the optimal configuration (and a zero thickness beam) are shown in Fig. 5. The solid line shows the peak power at the optimal electric field strength. This represents the maximum possible performance, but also requires that the quality factor be varied at each point. The zero

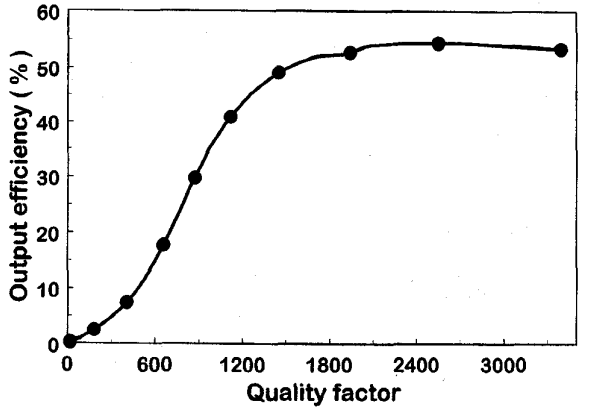

Fig. 4. The dependence of output efficiency on the output cavity quality factor (P_{in} = 800 W).

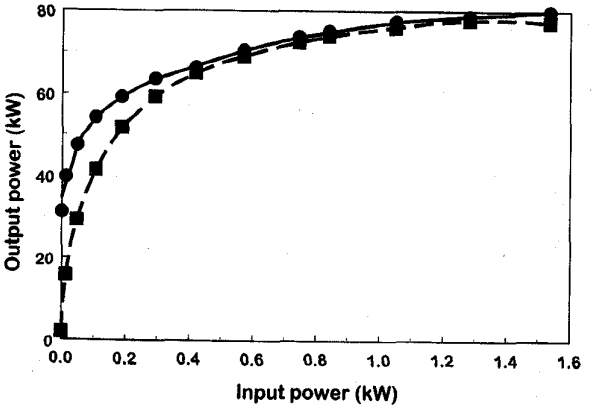

Fig. 5. System drive curves. The solid line shows the output efficiency at the optimal electric field strength. The dashed line gives the output efficiency for a constant quality factor (Q = 1825).

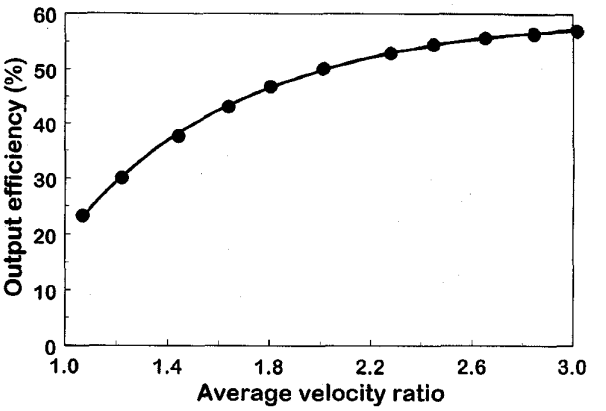

Fig. 6. The dependence of output efficiency on average velocity ratio.

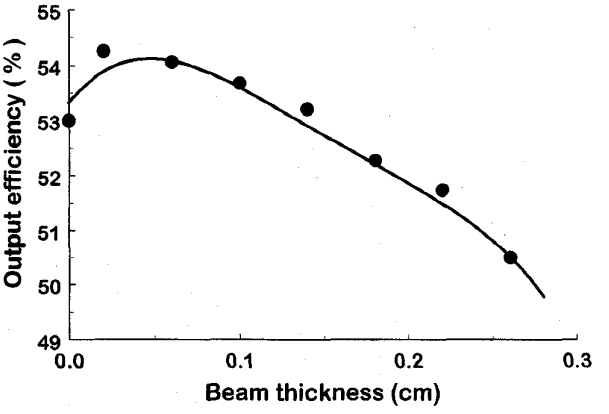

Fig. 7. The dependence of output efficiency on beam thickness.

drive efficiency is over 22% and requires an output quality factor of 3180. The second curve gives the output power for the original output cavity with a Q of 1825. Performance is poor at low drive powers, where the zero input efficiency is less than 2%. However, the two curves are quite similar near the maximum output power, which occurs for the latter curve at an input power of 1. 4 kW. The corresponding power and efficiency are 78 kW and 55.7% efficiency, respectively.

The dependence of output efficiency on the thin beam's average velocity ratio is given in Fig. 6. This ratio is modified solely by varying the magnetic field in the drift region. The phase and amplitude of the output cavity's electric field are optimized at each point. This again implies that the quality factor is adjusted to maximize output power. All other parameters, however, are held at their nominal values. The efficiency drops off fairly rapidly with decreasing velocity ratio, going to a level of about 23% at a velocity ratio near one. This result requires a quality factor of 8570. Efficiency only slowly increases above the nominal velocity ratio, approaching a level of 57% with a velocity ratio of three and a quality factor of 1635. This result would undoubtedly degrade with the introduction of finite beam thickness. On the other hand, performance could possibly be improved further if additional optimizations (e.g., cavity length adjustment) were performed.

The effect of beam thickness on efficiency at the nominal operating point has been examined in Fig. 7. The efficiency is fairly insensitive to beam thickness and the resulting velocity spread. For example, efficiency barely dips below 50% at a beam thickness of 0.26 cm and an axial velocity spread near 25%. Particles begin to hit the output cavity wall when the thickness exceeds 0.28 cm.

The results from the single particle code are confirmed using the (independent) gyroklystron code [40]. In these simulations, the prebunched beam shown in Fig. 3(b) and field profiles from the scattering matrix code are used as the input. The effect of magnetic field taper is presented in Fig. 8(a). The field amplitude and phase are adjusted at each value of magnetic taper to optimize the efficiency. The beam current is adjusted such that the required quality factor from the large signal code matches with the Q value from the scattering matrix code. It is important to note that the product of the beam current and Q is proportional to the square of field amplitude and inversely proportional to the efficiency. If the beam current is not within the acceptable range, then the amplitude and phase should be readjusted or the cavity should be redesigned with a different value of Q. The efficiency values plotted in Fig. 8(a), shown by the circles, correspond to 10% rms spread in the axial velocity. The corresponding values of optimum beam current are shown by the triangles. It can be seen that the efficiency is

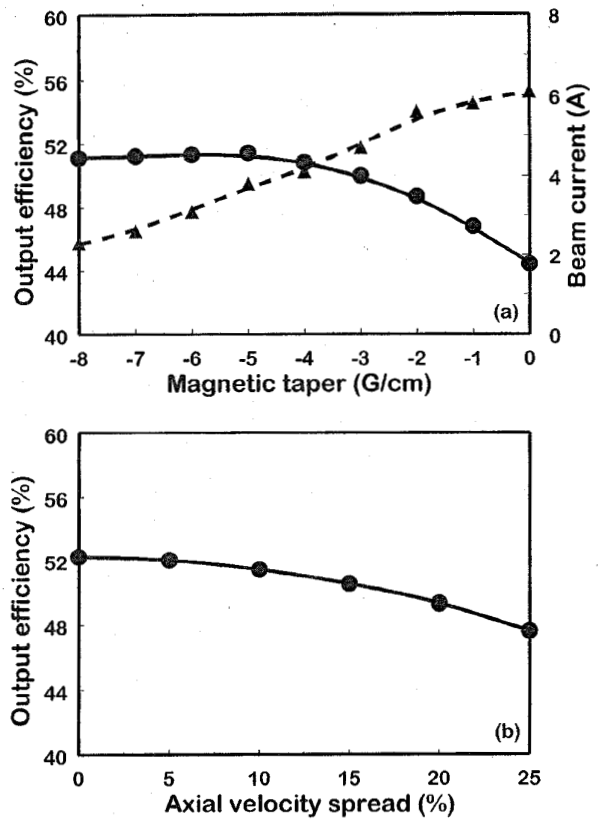

Fig. 8. Gyroklystron code results: (a) output efficiency (solid line) and optimal current (dashed line) as a function of magnetic field taper and (b) output efficiency as a function of velocity spread.

maximum for the magnetic taper value of -5 G/cm which is equivalent to a -3% taper. The beam current of 3.8 A matches well with design current of 4.0 A based on the single particle code. The magnetic taper improves the efficiency from 44.4% at zero taper to 51.4%. Higher magnetic tapers correspond to lower values of field amplitudes required to achieve maximum efficiency and hence lower values of optimum beam current. The optimum beam current (for a fixed value of $Q = 1825$) varies from 2.3 to 6.1 A for the magnetic taper of -8 to 0 G/cm. The corresponding output power level varies from 40 to 95 kW.

The effect of axial velocity spread on the design point is plotted in Fig. 8(b). This assumes that the beam is monoenergetic at the entrance of the output cavity. It can be seen from the figure that the output efficiency is above 50% for axial velocity rms spreads up to 15%. The decrease in efficiency with the velocity spread is very slow for this device as compared to second-harmonic gyrotrons or other devices. It is important to note that the velocity spread in the gyroklystron code is "placed" on the nominal beam distribution and thus is quite different from the spread computed by the two single particle codes. Nonetheless, the agreement between the two types of simulations is excellent.

The final simulation that we present utilizes an input cavity that is resonant in the TM_{010} mode at half the output frequency. This trivially satisfies the requirement in (1). The drift region length is doubled to conform to (2). The drive power is adjusted to introduce a similar energy spread into the beam. Most of the other parameters remain the same. All of the values that are adjusted are summarized in Table III; those not adjusted remain as in Table I. For a quality factor of about 2540, an electronic efficiency of 50.9% is achieved. This represents only a slight decrease ($\sim$2%) over the second-harmonic drive case. Furthermore, the reduced input power requirement, coupled with the higher quality factor and the lower stored energy boosts the large-signal gain to over 28 dB.

TABLE III
FIRST-HARMONIC DRIVE SYSTEM PARAMETERS

Input Cavity	
Drive frequency (GHz)	4.95
Operating mode	TM_{010}
Resistive Quality factor (Q)	3630
Radius (cm)	2.318
Length (cm)	0.40
Input drive power (W)	110
E_z at beam (kV/cm)	4.1
Drift region	
Cavity - cusp spacing (cm)	26
Total Δv_z (%)	11.8
Total $\Delta v_\perp$ (%)	1.7
Energy spread (%)	3.3
Output cavity	
Diffractive Q	2540
Power (kW)	71.3
Efficiency (%)	50.9
Gain (dB)	28.1
E_ϕ at beam (kV/cm)	44

IV. DISCUSSION

The novel concept of an axially prebunched low-voltage second-harmonic small-orbit gyrotron presented here promises reasonable gains and unprecedented efficiencies in a compact design. Because the beam is linearly streaming throughout most of the tube, this device is easily more stable than a comparable gyroklystron. The ability to use overmoded output cavities should enable these tubes to achieve higher powers than comparable klystrons.

The specific designs investigated here utilized a 35-kV 4-A beam to produce over 70 kW of power at 9.9 GHz via an axially coupled TE_{011} output cavity. Simulations were carried out with a single particle code which was modified to accept realistic cold-cavity field profiles from a scattering matrix code. The two-cavity gains with second- (TM_{020}) and first-harmonic (TM_{010}) input cavities were 20 and 28 dB, respectively. The simulated efficiency for the X-band input cavity system of 53% included nonideal effects due to finite beam thickness and cusp-width. The efficiency of the first-harmonic input system was only about 2% lower and required an output cavity Q about 39% higher than the previous design. The addition of one or more second-harmonic buncher cavities should allow for shorter drift regions, higher gain, and possibly higher efficiency. It should also minimize the performance discrepancies between the two input schemes.

One of the key differences between the axial bunching schemes for large- and small-orbit devices is the axial velocity spread resulting from the energy modulation. While the approximate expression for velocity spread (4) is the same for both cases, the effect of the input cavity's magnetic field appears to reduce the axial spread in large-orbit systems [34], but does little for the spread in small-orbit systems. This difference stems in part from the effect of each electron's radial displacement on the postcusp velocity ratio. Fortunately, this spread can often be minimized by choosing a drift length that is proportional to the axial periodicity of the beam's radial perturbation. It is also possible that the beam focusing of the electron gun could be designed to reduce the velocity spread. Additional work must be done on this concept to determine its viability.

Another concept which requires further investigation is the operation of prebunched small-orbit devices above the second harmonic. Third-harmonic operation was briefly simulated during this investigation with a (third-harmonic) TM_{020} input cavity and a TE_{021} output cavity, but no systematic study was undertaken. By varying the guiding center radius, we were able to fairly quickly find operating points with efficiencies exceeding 40%, however, the required output cavity quality factors were comparable to the resistive Q's of copper cavities. It is possible that operation was hindered by the induced axial velocity spread, because harmonic operation is increasingly more sensitive to such spread. However, it is also possible that further optimization would have resulted in high efficiency at a realistic operating point, particularly since the magnetic field resonance is quite narrow at low voltage. In systems that can tolerate higher beam voltages, the correspondingly broader magnetic field resonances should facilitate high harmonic operation.

A final question involves the effect of the input cavity's leakage fields on tube performance. If necessary, absorbers can be placed in the drift region to attenuate leakage power. However, there may still be some net effect on the beam's velocity modulation that should be investigated with a scattering matrix code which can model lossy dielectrics.

Because of the high quality factors of both cavities in this design, the instantaneous bandwidth of this device should be relatively small. However, we propose that this concept can readily be extended to a broad-band version. Because the beam is bunched with a TM_{0n} mode, the input cavity and drift tube region can be replaced by a helix (or some other slow wave) structure. By the same token, the output cavity can be replaced by a smooth-walled traveling wave section. This device should realize bandwidths comparable to traveling wave tubes (TWT's), achieve higher powers and efficiencies than conventional TWT's [41], and be more stable than gyro-TWT's [42]. The two regions will be naturally isolated from each other by the center plug of the iron pole piece (that is used to generate the nonadiabatic transition). Isolation should be further enhanced because the field patterns in each region are quite distinct.

In the future, we will attempt to investigate the theoretical questions left unanswered in the preceding few paragraphs. We also expect to work on an experimental investigation of this concept. We are in the process of building an experimental test bed which is energized by a 50-kV 20-A 5-μs pulse–line modulator. We have the capability to produce magnetic fields of about 2 kG over the required distance and are currently designing an electron gun compatible with the beam parameters of this design.

REFERENCES

[1] R. S. Symons and H. R. Jory, *Advances in Electronics and Electron Physics*, vol. 55, C. Marton, Ed. New York: Academic, 1981, ch. 1, p. 1.

[2] V. L. Granatstein, M. E. Read, and L. R. Barnett, *Infrared and Millimeter Waves*, vol. 5, K. Button, Ed. New York: Academic, 1981, ch. 5, p. 267.

[3] K. E. Kreischer, T. L. Grimm, W. C. Guss, A. W. Mobius, and R. J. Temkin, "Experimental study of a high-frequency megawatt gyrotron oscillator," *Phys. Fluids B*, vol. 2, pp. 640–646, 1990.

[4] K. Felch, C. Hess, H. Huey, E. Tongewaard, H. Jory, J. Neilson, R. Pendleton, and M. Tsirulnikov, "Recent long-pulse and high average power tests on a 140 GHz gyrotron," in *Proc. SPIE*, vol. 1514, pp. 315–317, 1990.

[5] B. Levush and T. M. Antonsen, "Mode competition and control in high-power gyrotron oscillators," *IEEE Trans. Plasma Sci.*, vol. 18, pp. 260–272, 1990.

[6] O. Dumbrajs and G. S. Nusinovich, "Cold-cavity and self-consistent approaches in the theory of mode competition in gyrotrons," *IEEE Trans. Plasma Sci.*, vol. 20, pp. 133–138, 1992.

[7] G. P. Saraph, T. M. Antonsen, B. Levush, and G. I. Lin, "Regions of stability of high-power gyrotron oscillators," *IEEE Trans. Plasma Sci.*, vol. 20, pp. 115–125, 1992.

[8] W. C. Guss, M. A. Basten, K. E. Kreischer, and R. J. Temkin, "Velocity spread measurements on a magnetron injection gun beam," *J. Appl. Phys.*, vol. 76, pp. 3237–3243, 1994.

[9] W. C. Guss, M. A. Basten, K. E. Kreischer, R. J. Temkin, T. M. Antonsen, S. Y. Cai, G. Saraph, and B. Levush, "Influence of sideband oscillations on gyrotron efficiency," *IEEE Trans. Plasma Sci.*, vol. 22, pp. 871–877, 1994.

[10] V. L. Bratman, N. S. Ginzburg, G. S. Nusinovich, M. I. Petelin, and P. S. Strelkov, "Relativistic gyrotrons and cyclotron autoresonance masers," *Int. J. Electron.*, vol. 51, pp. 541–567, 1981.

[11] K. D. Pendergast, B. G. Danly, R. J. Temkin, and J. S. Wurtele, "Self-consistent simulation of cyclotron autoresonance maser amplifiers," *IEEE Trans. Plasma Sci.*, vol. 16, pp. 122–128, 1988.

[12] V. L. Bratman and G. G. Denisov, "Cyclotron autoresonance masers—Recent experiments and prospects," *Int. J. Electron.*, vol. 72, pp. 969–981, 1992.

[13] G. F. Brand, Y. Idehara, T. Tatsukawa, and I. Ogawa, "Mode competition in a high harmonic gyrotron," *Int. J. Electron.*, vol. 72, pp. 745–758, 1992.

[14] W. Lawson, H. W. Matthews, M. K. E. Lee, J. P. Calame, J. Cheng, B. Hogan, P. E. Latham, V. L. Granatstein, and M. Reiser, "High power operation of a K-band second harmonic gyroklystron," *Phys. Rev. Lett.*, vol. 71, pp. 456–459, 1993.

[15] D. V. Kisel, G. S. Korablev, V. G. Navel'gev, M. I. Petelin, and Sh. E. Tsimring, "An experimental study of a gyrotron operating at the second harmonic of the cyclotron frequency with optimized distribution of the high-frequency field," *Radio Eng. Electron. Phys.*, vol. 19, pp. 95–100, 1974.

[16] B. G. Danly and R. J. Temkin, "Generalized nonlinear harmonic gyrotron theory," *Phys. Fluids*, vol. 29, pp. 561–567, 1986.

[17] P. Sprangle, "Excitation of electromagnetic waves from a rotating annular relativistic e-beam," *J. Appl. Phys.*, vol. 47, pp. 2935–2940, 1976.

[18] W. W. Destler, D. W. Hudgings, M. J. Rhee, S. Kawasaki, and V. L. Granatstein, "Experimental study of microwave generation and suppression in a nonneutral e-layer," *J. Appl. Phys.*, vol. 48, pp. 3291–3296, 1977.

[19] H. S. Uhm and R. C. Davidson, "Intense microwave generation by the negative-mass instability," *J. Appl. Phys.*, vol. 49, pp. 593–598, 1978.

[20] W. W. Destler, H. Romero, C. D. Striffler, R. L. Weiler, and W. Namkung, "Intense microwave generation from a nonneutral rotating E layer," *J. Appl. Phys.*, vol. 52, pp. 2740–2749, 1981.

[21] W. W. Destler, R. L. Weiler, and C. D. Striffler, "High-power microwave generation from a rotating E layer in a magnetron-type waveguide," *Appl. Phys. Lett.*, vol. 38, pp. 570–572, 1981.

[22] Y. Y. Lau and L. R. Barnett, "Theory of a low magnetic field gyrotron (gyromagnetron)," *Int. J. Infrared Millimeter Waves*, vol. 3, pp. 619–643, 1982.
[23] W. W. Destler, R. Kulkarni, C. D. Striffler, and R. L. Weiler, "Microwave generation from rotating electron beams in magnetron-type waveguides," *J. Appl. Phys.*, vol. 54, pp. 4152–4162, 1983.
[24] W. Namkung, "Observation of microwave generation from a cusptron device," *Phys. Fluids*, vol. 27, pp. 329–330, 1984.
[25] K. R. Chu and D. Dialetis, "Theory of harmonic gyrotron oscillator with slotted resonant structure," *Int. J. Infrared Millimeter Waves*, vol. 5, pp. 37–56, 1984.
[26] W. Lawson, W. W. Destler, and C. D. Striffler, "High-power microwave generation from a large-orbit gyrotron in vane and hole-and-slot conducting wall geometries," *IEEE Trans. Plasma Sci.*, vol. PS-13, pp. 444–453, 1985.
[27] E. Chojnacki, W. W. Destler, W. Lawson, and W. Namkung, "Studies of microwave radiation from a non-relativistic rotating electron beam in a multiresonator magnetron cavity," *J. Appl. Phys.*, vol. 61, pp. 1268–1275, 1987.
[28] H. P. Bluem, P. E. Latham, W. Lawson, and C. D. Striffler, "Single-particle motion in a large-orbit gyrotron," *IEEE Trans. Microwave Theory Tech.*, vol. MTT-35, pp. 946–955, 1987.
[29] W. W. Destler, E. Chojnacki, R. F. Heoberling, W. Lawson, A. Singh, and C. D. Striffler, "High-power microwave generation from large-orbit devices," *IEEE Trans. Plasma Sci.*, vol. 16, pp. 71–89, 1988.
[30] W. W. Destler, K. Irwin, W. Lawson, J. Rodgers, Z. Segalov, E. P. Scannell, and S. T. Spang, "Intense-beam fundamental mode large-orbit gyrotron studies," *J. Appl. Phys.*, vol. 66, pp. 4089–4094, 1989.
[31] C. S. Kou, D. B. McDermott, N. C. Luhmann, Jr., and K. R. Chu, "Prebunched high-harmonic gyrotron," *IEEE Trans. Plasma Sci.*, vol. 18, pp. 343–349, 1990.
[32] K. Irwin, W. W. Destler, W. Lawson, J. Rodgers, E. P. Scannel, and S. T. Spang, "Second generation, high power, fundamental mode large-orbit gyrotron experiments," *J. Appl. Phys.*, vol. 69, pp. 627–631, 1991.
[33] K. K. Tiong and S. P. Kuo, "Operation of a high harmonic cusptron oscillator," *Int. J. Electron.*, vol. 70, pp. 815–821, 1991.
[34] W. Lawson and W. W. Destler, "The axially modulated, cusp-injected, large-orbit gyrotron amplifier," *IEEE Trans. Plasma Sci.*, vol. 22, pp. 895–901, 1994.
[35] M. J. Rhee and W. W. Destler, "Relativistic electron dynamics in a cusped magnetic field," *Phys. Fluids*, vol. 17, pp. 1574–1581, 1974.
[36] W. Lawson and P. E. Latham, "The design of a small-orbit/large-orbit gyroklystron experiment," *J. Appl. Phys.*, vol. 61, pp. 519–528, 1987.
[37] R. E. Collin, *Foundations for Microwave Engineering*. New York: McGraw-Hill, 1966, pp. 462–470.
[38] J. Neilson, P. E. Latham, M. Caplan, and W. Lawson, "Determination of the resonant frequencies in a complex cavity using the scattering matrix formulation," *IEEE Trans. Microwave Theory Tech.*, vol. 37, pp. 1165–1170, 1989.
[39] W. Lawson and P. E. Latham, "The scattering matrix formulation for overmoded coaxial cavities," *IEEE Trans. Microwave Theory Tech.*, vol. 40, pp. 1973–1976, 1992.
[40] K. R. Chu, V. L. Granatstein, P. E. Latham, W. Lawson, and C. D. Striffler, "A 30-MW gyroklystron-amplifier design for high-energy linear accelerators," *IEEE Trans. Plasma Sci.*, vol. PS-13, pp. 424–434, 1985.
[41] D. Shiffler, J. A. Nation, and G. S. Kerslick, "A high-power, travelling wave tube amplifier," *IEEE Trans. Plasma Sci.*, vol. 18, pp. 546–552, 1990.
[42] K. R. Chu, L. R. Barnett, W. K. Lau, L. H. Chang, and H. T. Chen, "A wide-band millimeter-wave gyrotron travelling-wave amplifier experiment," *IEEE Trans. Electron Devices*, vol. 37, pp. 1557–1560, 1990.

Wes Lawson (S'84–M'85–SM'95), for a photograph and biography, see this issue, p. 665.

A. Grigoropoulos, photograph and biography not available at the time of publication.

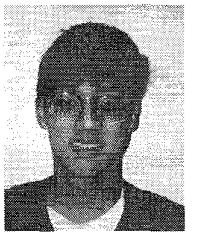

A. Liu was born in Columbia, MD in 1976. For the past year he has been working at the Institute for Plasma Research, University of Maryland, College Park, as an Undergraduate Research Assistant while pursuing the B.S. degree in electrical engineering at the University of Maryland.

Girish P. Saraph (S'91–M'93), for a photograph and biography, see this issue, p. 677.

John Rodgers received the B.S.E.E. degree from the University of Maryland, College Park, in 1987.

He served in the U.S. Navy from 1975 to 1981 as a Communications and Radar Electronics Technician. From 1981 to 1984 he was with the Space Department of the Johns Hopkins Applied Physics Laboratory. Since 1987 he has worked at the University of Marlyand as a Faculty Research Assistant in the Laboratory for Plasma Research.

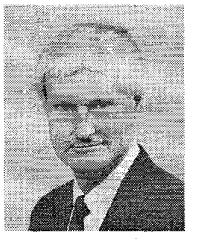

William W. Destler (M'84–SM'90–F'92) received the B.S. degree from the Stevens Institute of Technology, Hoboken, NJ, in 1968 and the Ph.D. degree from Cornell University, Ithaca, NY, in 1972.

He is presently Dean of Engineering at the University of Maryland at College Park. His research interests have been primarily in the areas of high-power microwave sources and advanced accelerator technology, and he is the author or co-author of over 100 research papers on these and related topics.

Dr. Destler is the recipient of numerous awards for teaching excellence, including the 1989 AT&T/ASEE Award for Excellence in Engineering Education for the Mid-Atlantic States. He is a Fellow of the American Physical Society.